Pergamon

Int. J. Heat Mass Transfer. Vol. 38, No. 14, pp. 2569–2581, 1995

0017–9310/95 $9.50+0.00

0017–9310(95)00013–5

Optical properties of thick, turbid media from picosecond time-resolved light scattering measurements

M. Q. BREWSTER†
Department of Mechanical and Industrial Engineering, University of Illinois, Urbana, IL 61801, U.S.A.

and

Y. YAMADA
Mechanical Engineering Laboratory, AIST-MITI, 1-2 Namiki, Tsukuba, Ibaraki 305, Japan

(*Received* 11 *July* 1994 *and in final form* 10 *December* 1994)

Abstract—A computational and experimental investigation is reported regarding the feasibility of determining optical properties of turbid media from picosecond (PS) time-resolved light scattering measurements in conjunction with diffusion theory predictions, Monte Carlo simulations, and other appropriate optical measurements. Picosecond time-resolved transmission measurements were performed using aqueous latex particle suspensions with and without absorbing dye. Monte Carlo simulations were also performed to aid in determining limitations of the approach as well as suitable measurement parameters. The system of interest was an optically thick plane-parallel, homogeneous slab consisting of an absorbing, anisotropic scattering medium subject to collimated, pulsed incident radiation. The results of comparing Monte Carlo and diffusion theory predictions showed that important pulse parameters, such as long-time asymptotic log slope and RMS pulse width, are given by diffusion theory analytical expressions with enough accuracy to be useful for determining the unknown optical properties of the medium from time-resolved scattering measurements. These findings were verified using PS time-resolved transmission measurements on aqueous latex particle suspensions. It was also found that the albedo criterion for application of diffusion theory to time-dependent scattering may be much less restrictive than is usually reported (weak absorption or albedo near one is not necessary).

1. INTRODUCTION

Picosecond (PS) time-resolved light scattering is a promising method for determining optical properties of absorbing-scattering media. Many of the difficulties of traditional time-integrated methods for determining optical properties can be overcome with time-resolved measurements. These difficulties include the need for signal calibration, collection of light over a specified solid angle, and restrictions with regard to incident beam and scattering medium geometry (e.g. beam width $\gg$ medium thickness, etc.). Time-resolved techniques are therefore particularly useful in situations where sample manipulation is not easily accomplished and remote or *in-situ* measurements are necessary. Possible applications of time-resolved light scattering are high power laser plumes and plasmas, particle-laden flames, atmospheric aerosols and biological tissues. Of these, biological tissues (which are relatively optically thick) have received the most attention recently [1–3] with regard to time-resolved scattering measurements.

Several recent studies have reported on the feasibility of determining optical properties of thick, turbid media from time-resolved light scattering measurements in conjunction with simple analytical predictions of diffusion theory. Patterson *et al.* [4] showed that the near infrared optical properties of biological tissue (human calf muscle) could be obtained from temporal characteristics of the back-scattered (i.e. reflected) pulse corresponding to a time- and space-wise narrow incident pulse of laser light. Reflected light was measured at a distance of 40 mm (approximately 34 mean free photon pathlengths) from the source to ensure validity of the diffusion solution at the point of measurement. An instantaneous, isotropic, point-source was used in the diffusion solution to simulate the incident laser pulse. The measured time of maximum signal (t_m) and the long-time, asymptotic log slope (ALS) of the reflected pulse were used in conjunction with diffusion theory to obtain reasonable estimates of the absorption coefficient (K_a) and equivalent isotropic scattering coefficient ($K_{sI} = K_s(1-g)$). The possibility of obtaining both optical coefficients from a single time-resolved, spatially integrated transmission measurement was also suggested. Diffusion theory predictions were shown to match the spatially integrated transmitted pulse shape of Monte Carlo simulations reasonably well.

NOMENCLATURE

ALS asymptotic log slope, equation (1)
c_o speed of light in vacuum or constant in equation (14)
d particle diameter
FWHM full-width, half-maximum
f_v particle volume fraction
g asymmetry parameter
K absorption, extinction, or scattering coefficient
k absorption index
L slab thickness
m see equation (2)
n refractive index
p scattering phase function
Q absorption, extinction, or scattering efficiency
R time-resolved hemispherical reflectance
RMSW root-mean-square width
T time-resolved hemispherical transmittance
t time
t_o L/c, time for ballistic transport across slab L
t_m time of maximum signal
x $\pi d/\lambda$, particle size parameter
y see equation (13).

Greek symbols
β $3\omega_I\tau_I$
θ single scattering or slab polar angle
λ_o wavelength in vacuum
η $3(1-g)$
τ optical depth
ω single scattering albedo.

Subscripts
a absorption
c critical, characteristic, or speed of light
e extinction (scattering plus absorption)
I effective isotropic scattering value
p particle
s scattering
w water.

Superscripts
′ normalized, dimensionless.

Using the semi-infinite diffusion theory model of Patterson *et al.* [4], Madsen *et al.* [5] conducted a more extensive comparison with experimental data with Intralipid solution as the scattering medium and India ink as an absorbing agent. The properties K_a and K_{sI} were obtained by curve-fitting the diffusion theory time-resolved, spatially local reflectance predictions to measured data. For sufficiently large samples generally good agreement was found with independent, steady-state measured values, although there was a tendency for K_a to be slightly underestimated and K_{sI} overestimated by the time-resolved technique. The cause of these systematic deviations was not identified, although finite geometry effects were ruled out. Some of the difficulty may have been due to unwanted scattering by the ink particles. It was recommended that further studies be done to establish the bounds of applicability of the simple semi-infinite diffusion model to finite samples and that experimental systems with well-defined optical properties be used, such as latex spheres.

In a recent, extensive experimental investigation, Zaccanti *et al.* [6] used aqueous latex particle suspensions and streak camera detection to investigate the parameters that influence transmitted pulse shape in thick, turbid media. They showed experimentally that, as predicted by diffusion theory, the parameters that most influence transmitted pulse shape are K_{sI} and K_a (or equivalently isotropic optical thickness $\tau_I = (K_{sI}+K_a)L$ and isotropic albedo $\omega_I = K_{sI}/(K_{sI}+K_a)$). For example, their results showed that for a wide variety of different particle sizes, two statistical measures of pulse shape, t_m and FWHM (full width at half maximum), both correlated closely with τ_I in spite of widely varying values of actual optical thickness τ. In fact, for $\tau_I > 10$, both t_m and FWHM increased linearly with τ_I. Thus they concluded that it is quite feasible to obtain the optical properties of dense, turbid media from appropriate time-resolved transmission measurements. They point out, however, that a key necessary ingredient is a knowledge of the relationship between the output pulse shape parameters (e.g. ALS, t_m, FWHM, etc.) and the fundamental optical properties such as τ_I and ω_I. Comparisons with the diffusion approximation solution of Ito and Furutsu [7] for a plane incident wave (wide beam) and hemispherical detection showed that the diffusion theory predictions for pulse width (e.g. FWHM) were significantly wider than the measurements. Since the experiments used a narrow beam and in-line, narrow field-of-view detection, this disagreement was attributed as being possibly due to configuration and boundary condition differences. A later analysis of the narrow incident beam case by Ito [8] confirmed that this indeed may be true. Ito's narrow beam results showed the transmitted pulse width to be a function of radial position relative to the incident beam location. For radial locations near the axis of the incident beam the pulse width would be less than the corresponding pulse width for a plane wave while the opposite holds for locations far from the axis. For radially integrated measurements of the

transmitted pulse, the far- and near-axis regions would cancel each other and the pulse width would be the same as for the plane wave case.

These past studies provide some evidence that suggests diffusion theory may be satisfactory for extracting optical properties of dense, turbid media from time-resolved light scattering measurements. However, considerations such as beam width, detector location and solid angle, type of output pulse (transmitted or reflected), refractive index mismatching, etc. may be necessary. A more complete understanding of the sensitivity of measurable pulse parameters to various experimental conditions and theoretical assumptions is needed before time-resolved light scattering can be fully exploited.

The object of this study was to further investigate the feasibility of determining optical properties of turbid media from time-resolved light scattering measurements in conjunction with diffusion theory predictions, Monte Carlo simulations, and other appropriate optical measurements. Picosecond time-resolved transmission measurements were performed using aqueous latex particle suspensions with and without absorbing dye. Monte Carlo simulations were also performed to aid in determining limitations of the approach as well as suitable measurement parameters. The system of interest is a plane-parallel, homogeneous slab consisting of an absorbing, anisotropic scattering medium subject to collimated, pulsed incident radiation. The slab optical thickness is restricted to relatively large values ($\tau_1 > 10$) such that diffusive or incoherent scattering dominates as opposed to coherent or ballistic scattering (see e.g. refs. [9] or [10]).

2. OPTICAL PROPERTIES

The optical properties of interest in this study can be expressed in various equivalent forms. The basic properties consist of the following set of three: (1) scattering coefficient K_s, (2) absorption coefficient K_a or extinction coefficient $K_e = K_a + K_s$ and (3) asymmetry parameter, g. (In lieu of the full angular phase function $p(\theta)$, which contains too much detailed information, the single scattering asymmetry parameter g is used.) A non-dimensional set of parameters that is basically equivalent to the set above but includes L is as follows: (1) single scattering albedo $\omega = K_s/K_e$, (2) slab optical thickness $\tau = K_e L$ and (3) asymmetry parameter, g.

Under conditions that satisfy the diffusion approximation, it is convenient to transform the first two of these to equivalent isotropic scattering properties. In terms of dimensional (volume) coefficients, these properties are (1) isotropic scattering coefficient $K_{sI} = K_s(1-g)$ and (2) absorption coefficient K_a or isotropic extinction coefficient $K_{eI} = K_{sI} + K_a = K_e(1-\omega g)$. The corresponding non-dimensional properties are (1) isotropic albedo $\omega_I = K_{sI}/K_{eI} = \omega(1-g)/(1-\omega g)$ and (2) isotropic optical thickness $\tau_I = K_{eI}L = \tau(1-\omega g) = \tau(1-g)/[1-g(1-\omega_I)]$. The convenience of this transformation comes from the fact that under certain conditions the set of three anisotropic parameters can be replaced by the two equivalent isotropic parameters. The effect of anisotropic scattering is incorporated completely into the first two parameters. Such conditions include point or otherwise isotropic sources (e.g. thermal emission) and long-time response to pulsed incident radiation.

Several conditions are usually given as being necessary for establishment of radiative diffusion: (1) large optical thickness of the medium, (2) long times and (3) spatial locations far from sources. An additional restriction that is also often mentioned is that of high albedo (weak absorption) (Ishimaru [11]; Patterson *et al.* [4]] but the limiting values of albedo have not been clearly defined in a general way. It is quite possible that the allowable albedo could vary considerably depending on the desired quantity (e.g. instantaneous local fluence rate as opposed to long-time decay rate of scattered radiation, etc.).

The simplest approach to characterizing the optical properties of a turbid medium is to try to do so first in terms of the equivalent isotropic properties τ_I and ω_I. In theory, two measurable output functions $F(\tau_I, \omega_I)$ and $G(\tau_I, \omega_I)$ with non-zero Jacobian (i.e. F and G are not uniquely related; $F \neq F(G)$ and $G \neq G(F)$) can be used to determine τ_I and ω_I by mathematical inversion. Measurable functions which are candidates for F and G are considered below.

3. OUTPUT PULSE PARAMETERS

Various output pulse parameters can be considered as candidate functions of τ_I and ω_I. These include ALS, t_m, FWHM and RMSW (root-mean-square width) as applied to either the reflected or transmitted pulse. The mathematical definitions of ALS and RMSW (in terms of transmitted pulse) are given below, where T is time-resolved, hemispherical transmittance.

$$\mathrm{ALS} = \lim_{t_I' \to \infty} -\frac{\mathrm{d}\ln T}{\mathrm{d}t_I'} = 2.303 m t_o/\tau_I \tag{1}$$

where

$$t_I' = \frac{t}{t_{cI}};\ t_{cI} = \frac{1}{K_{eI}c} = t_o/\tau_I;\ m = \lim_{t \to \infty} -\frac{\mathrm{d}\log T}{\mathrm{d}t} \tag{2}$$

$$\mathrm{RMSW} = \frac{\langle \Delta t^2 \rangle^{1/2}}{t_o};\ \langle \Delta t^2 \rangle = \langle t^2 \rangle - \langle t \rangle^2; \tag{3}$$

$$\langle t^n \rangle = \frac{\int_{-\infty}^{\infty} t^n T(t)\,\mathrm{d}t}{\int_{-\infty}^{\infty} T(t)\,\mathrm{d}t},\ n = 1, 2, 3 \ldots$$

The first expression for ALS can be viewed as a fundamental definition (based on diffusion theory considerations) and the second expression as a more prac-

tical working formula for obtaining ALS from time-resolved scattering data. The slope m is the dimensional, base 10 counterpart of ALS and t_o ($= L/c$) is the time for ballistic transport across the slab.

With proper consideration it should be possible to select a combination of output pulse parameters which are both easily measurable and mathematically independent such that τ_I and ω_I can be obtained from a time-resolved measurement of the output pulse corresponding to a narrow input pulse. This assumes of course that a connecting theory or set of relations between the output functions and the optical properties (τ_I and ω_I) is available. Selection of the appropriate parameters will depend on the nature of the particular system of interest and must include considerations of the type and variety of optical measurements that can be made, the available time-resolution of the optical system, and signal-to-noise ratio. With τ_I and ω_I having been obtained in this manner it would often be possible to obtain the third optical property (g, and thus the full anisotropic set) from a measurement of the time-integrated, direct, unscattered transmittance, $\exp(-\tau)$, on a relatively optically thin sample of the medium [12].

4. DIFFUSION THEORY (PLANE-WAVE) RESULTS

In this section the pertinent results from diffusion theory are summarized. The solution to the problem of scattering of a plane-wave incident pulse by an optically thick slab was obtained by Ito and Furutsu [7]. The expressions for time-resolved hemispherical reflectance $R(t)$ and transmittance $T(t)$ expressed in the isotropic parameter notation are as follows (see equations (35) and (40) of ref. [7]).

$$t_{cI}R(t_I', g, \tau_I, \omega_I) = \frac{3\omega_I}{\eta}\exp[-(1-\omega_I)t_I']\sum_{n=1}^{\infty}\exp[-3\omega_I s_n^2 t_I'/\beta^2] \times\left\{a_{on}+(-1)^n b_{on}\exp\left(-\frac{\beta}{\eta}+\frac{s_n^2}{\beta}\right)\right\} \quad (4)$$

$$t_{cI}T(t_I', g, \tau_I, \omega_I) = \frac{3\omega_I}{\eta}\exp[-(1-\omega_I)t_I']\sum_{n=1}^{\infty}\exp[-3\omega_I s_n^2 t_I'/\beta^2] \times\left\{(-1)^{n-1}a_{on}-b_{on}\exp\left(-\frac{\beta}{\eta}+\frac{s_n^2}{\beta}\right)\right\} \quad (5)$$

where

$$\eta = 3(1-g);\ \beta = 3\omega_I\tau_I \quad (6)$$

$$s_n \approx n\pi\left(1-\frac{2}{n\pi}\tan^{-1}\frac{2n\pi}{\beta}\right),\ n = 1, 2, 3, \ldots, \quad (7)$$

$$a_{on} = \frac{[(1/2+1/\eta)\beta^2 - s_n^2]s_n^2}{[\beta^3/4+\beta^2+\beta s_n^2][s_n^2+(\beta/\eta - s_n^2/\beta)^2]} \quad (8)$$

$$b_{on} = \frac{[(-1/2+1/\eta)\beta^2 - s_n^2]s_n^2}{[\beta^3/4+\beta^2+\beta s_n^2][s_n^2+(\beta/\eta - s_n^2/\beta)^2]}. \quad (9)$$

This solution is valid for $\beta \gg 1$ which is generally considered as being accomplished by conditions of weak absorption $\omega_I \to 1$ and large optical thickness $\tau_I \gg 1$. At long times both R and T approach the same expression

$$t_{cI}R(t_I', g, \tau_I, \omega_I) = t_{cI}T(t_I', g, \tau_I, \omega_I) = \frac{3\omega_I a_{o1}}{\eta}\exp[-(1-\omega_I)t_I' - 3\omega_I s_1^2 t_I'/\beta^2];\ t_I' \to \infty \quad (10)$$

from which the asymptotic log slope can be obtained as

$$\mathrm{ALS}(\tau_I, \omega_I) = (1-\omega_I) + \frac{3\omega_I\pi^2}{\beta^2}\left(1-\frac{2}{\pi}\tan^{-1}\left(\frac{2\pi}{\beta}\right)\right)^2. \quad (11)$$

The pulse width is given by a complex analytical expression which has the following power series expansion (see equation (61) of ref. [7]).

$$(\mathrm{RMSW})^2 = c_o - c_1 y + c_2 y^2 + \ldots, \quad (12)$$

where

$$y = \frac{1-\omega_I}{3\omega_I} \quad (13)$$

$$c_o = (\beta+4)^{-2}\left(\tfrac{1}{90}\beta^4+\tfrac{4}{15}\beta^3+\tfrac{8}{3}\beta^2+\tfrac{32}{3}\beta+16\right) \quad (14)$$

$$c_1 = \beta^2(\beta+4)^{-3}\left(\tfrac{2}{945}\beta^5+\tfrac{8}{105}\beta^4+\tfrac{128}{105}\beta^3+\tfrac{32}{3}\beta^2+\tfrac{256}{5}\beta+128+128/\beta\right) \quad (15)$$

$$c_2 = \beta^4(\beta+4)^{-4}\left(\tfrac{1}{3150}\beta^6+\tfrac{8}{525}\beta^5+\tfrac{176}{525}\beta^4+\tfrac{4096}{945}\beta^3+\tfrac{3712}{105}\beta^2+\tfrac{1280}{7}\beta+\tfrac{8704}{15}+1024/\beta+768/\beta^2\right). \quad (16)$$

The first three terms of this expansion are accurate in the range $\beta y^{1/2} \leqslant 1$. Complete evaluation of these results requires comparison with an exact solution of the problem. In the present work, Monte Carlo calculations are used for this purpose. The results of this comparison are discussed in the following sections.

5. MONTE CARLO RESULTS

Monte Carlo simulations (see e.g. ref. [13] for discussion of basic Monte Carlo approach) were conducted to determine more extensive information that is not available from simple diffusion theory and to investigate conditions when diffusion theory predictions can be expected to be accurate. Conditions of interest that generally fall outside the descriptive domain of diffusion theory include short time behavior, the effect of anisotropic scattering, and geometric variations such as detector field-of-view. The parameters used in the simulations were selected to

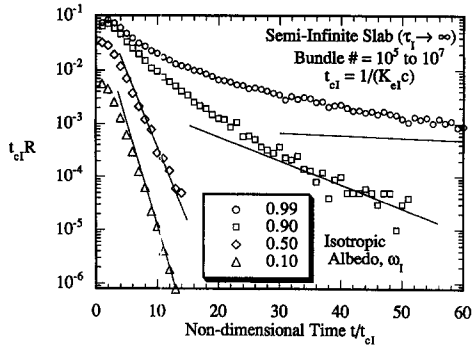

Fig. 1. Effect of albedo on time-resolved reflectance for semi-infinite slab with plane-wave, pulsed irradiation and isotropic scattering; symbols are Monte Carlo results; lines are diffusion theory predictions of ALS.

match those of 10 and 20 mm path length experimental scattering cells with aqueous latex water suspensions when possible. The results of these simulations are considered according to the effect of various parameters and assumptions as follows: albedo, optical thickness, anisotropic scattering, and detector field-of-view.

5.1. *Effect of albedo*

The effect of albedo is investigated using the case of a semi-infinite slab with isotropic scattering and a pulse of collimated irradiation at time $t = 0$. The results for non-dimensional, time-resolved reflectance ($t_{cl}R$) as a function of non-dimensional time are shown in Fig. 1. The Monte Carlo results in Fig. 1 (symbols) show that R, which starts at zero at $t = 0$, rises very rapidly to a peak and then decays relatively slowly. This decay rate, i.e. the asymptotic log slope (ALS), is the main feature of interest in Fig. 1. (It is shown subsequently that in the long-time domain, equivalent isotropic and anisotropic scattering results are the same so it is sufficient for the purposes of examining the ALS to consider only isotropic scattering.) Figure 1 also shows the corresponding ALS predicted from diffusion theory (straight lines). It can be seen that as the albedo increases the magnitude of ALS decreases according to the diffusion theory prediction for a semi-infinite slab

$$\text{ALS}\,(\tau_1 \to \infty) = (1-\omega_1). \tag{17}$$

It can be seen that the agreement of diffusion theory predictions for ALS with the Monte Carlo results is very good, even for the lower albedo cases. This agreement at low albedos is somewhat surprising in light of the general restriction of diffusion theory to high albedos ($\omega_1 \to 1$). Perhaps the reason for good agreement in this case is related to the fact that this case represents the long-time response to a short incident pulse as opposed to the short-time response to a pulse or the time-independent (i.e. steady-state) response to a steady input. In the latter cases the fluence rates at the boundary are much larger and therefore a stricter limit on albedo is necessary for accurate diffusion theory results (see ref. [11]). This finding also agrees with a recent report by Furutsu and Yamada [14] that the albedo criterion for the diffusion approximation is much less restrictive under time-dependent scattering conditions than under time-independent conditions (see also ref. [15]). (Reference [14] also corrects a common misconception regarding the diffusion coefficient in the presence of absorption and shows that $D = 1/[3K_{sl}]$ and not $1/[3(K_{sl}+K_a)]$ even when $K_a \neq 0$.) It can also be seen in Fig. 1 that as albedo increases the time required to reach asymptotic behavior increases. For example, at $\omega_1 = 0.99$, ALS is not reached until non-dimensional time reaches a value of about 400 (not shown in Fig. 1).

The important implication of the results for the semi-infinite medium is that the isotropic albedo (more accurately, the absorption coefficient) can quite easily be determined from a relatively simple time-resolved back-scattering measurement. The primary requirement of this measurement is to be able to maintain low enough noise to signal ratio at sufficiently long times to accurately measure the asymptotic log slope. Because the data of interest are often taken at long times (10^2–10^3 ps for high albedos), it may be possible to use relatively wide input pulses (tens of ps) without a need for deconvoluting the data. Another great advantage is that the asymptotic log slope is independent of the magnitude of the reflectance signal so calibration of the scattering signal magnitude is not necessary. Furthermore, ALS is not dependent on an accurate knowledge of the time origin (pulse occurrence) so time synchronization between the input pulse and scattered light is not necessary. Also, it is not actually necessary to use a broad, collimated input beam or to collect scattered light over all directions. It is sufficient to use any input beam (e.g. narrow-collimated laser) and collect scattered light over only a limited solid angle at any direction (so long as sufficient signal is obtained at long times). Any variety of light input and output geometries gives the same asymptotic log slope (see e.g. ref. [16]). The reason for this is that the asymptotic state is the state where photons have undergone extensive multiple scattering and have acquired a nearly isotropic directional distribution. The photons measured at these times leave the medium via diffusion from the interior toward the boundaries (in the case of a finite slab this means the transmittance also gives the same signal as the reflectance). Thus, the time variation of these long-time signals is independent of whether the photons were introduced into the medium via a broad beam or a narrow beam, and independent of direction and solid angle of collection. These simplifications offer significant experimental advantages over time-averaged techniques for measuring the albedo of a semi-infinite medium.

5.2. *Effect of optical thickness*

The influence of finite slab thickness on time-resolved reflectance and transmittance is shown in

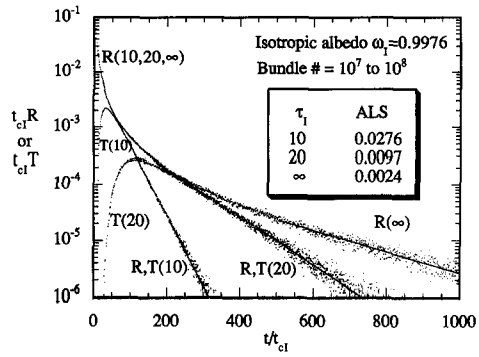

Fig. 2. Effect of optical thickness on time-resolved reflectance and transmittance for slab with plane-wave, pulsed irradiation and isotropic scattering (albedo = 0.9976); symbols are Monte Carlo results; lines are diffusion theory predictions of ALS.

Fig. 2 for isotropic scattering, a pulse of collimated irradiation, and a fixed albedo of 0.9976. The semi-infinite case $R(\infty)$ shows a time-resolved reflectivity similar to that of the high albedo (0.99) case of Fig. 1. For non-dimensional times greater than about 500 the log slope of $R(\infty)$ approaches the value 0.0024, in agreement with diffusion theory (shown by a straight line). By definition, the transmittance for this case is zero. The results for two finite slab optical thicknesses are also shown in Fig. 2 and designated as $\tau_1 = 10$ and 20 (the precise values are 9.922 and 19.844). For these two cases transmittance ($T(10)$, $T(20)$) is shown in addition to reflectance. Like the reflectance, transmittance also starts at zero and reaches a peak relatively rapidly. One difference between T and R is that T necessarily remains zero until after the time necessary for direct, unscattered photon transit across the slab ($t_o = L/c = \tau_1 t_{cI}$). Another noticeable difference, at least for these still relatively optically thick conditions, is that the peak T values occur at later times and with much lower magnitudes than the peak R values. It is interesting to note that for short times (up until about $t/t_{cI} = 60$ in Fig. 2) all three cases give essentially the same reflectance, $R(10,20,\infty)$. This is because the earliest reflected photons are back-scattered from the surface region near where photons are incident and thus the presence or absence of participating medium beyond about 10 mean free photon paths is not detectable in the R trace. However, for finite slab thicknesses, the R curves eventually deviate from the $R(\infty)$ curve and merge with the corresponding T curves. Interestingly, the point of departure of $R(10)$ (or $R(20)$) from $R(\infty)$ occurs at about the same point as the merger with $T(10)$ (or $T(20)$). This departure–merger point defines the onset of the asymptotic region for a given optical thickness. For $\tau_1 = 10$, the onset of asymptotic behavior occurs at about $t/t_{cI} = 60$ and for $\tau_1 = 20$ it occurs at about $t/t_{cI} = 250$. Beyond the merger point the $\log(R, T)$ curves decay at a constant rate. Figure 2 shows that the magnitude of the asymptotic log slope depends on optical thickness. As τ_1 decreases the magnitude of ALS increases. The values of ALS are 0.0276 and 0.0097 for $\tau_1 = 10$ and 20, respectively. These values are in agreement with those predicted from diffusion theory.

It is interesting also to note briefly the behavior of R for the non-absorbing case of $\omega = 1.000$ (although such a case is only an academic curiosity and never occurs in nature, even for visible light scattered by water droplets in air or latex particles in water). In this case diffusion theory predicts that for a semi-infinite medium $R(\infty)$ would continue approaching zero along the $t^{-3/2}$ trajectory (the same trajectory displayed by $R(\infty)$ in Fig. 2 between non-dimensional times of approximately 10 and 100). No matter how long the time, without absorption, $R(\infty)$ would never reach a constant asymptotic log slope, as is always the case with absorption ($\omega < 1.000$). Thus it is clear that either of two conditions is sufficient to cause R to approach a constant asymptotic log slope: (1) a slight (even infinitesimal) degree of absorption; and (2) finite medium optical thickness, as pointed out by Ito and Furutsu [7].

5.3. *Effect of anisotropic scattering*

Anisotropic scattering was investigated using Monte Carlo simulations of time-resolved scattering in conjunction with the Heyney–Greenstein (HG) phase function.

$$p(\cos\theta) = (1-g^2)[1+g^2-2g\cos\theta]^{-3/2}. \quad (18)$$

The HG phase function was selected here primarily for its simple analytic form which can easily be converted to a cumulative probability function for Monte Carlo computations.

$$\frac{1}{2}\int_{\cos\theta}^{1} p(\cos\theta')\,\mathrm{d}(\cos\theta') = (1-g^2)[(1-g)^{-1} - (1+g^2-2g\cos\theta)^{-1/2}]/(2g). \quad (19)$$

Many previous studies have reported satisfactory predictions with the HG phase function, although at least one study [17] has claimed that the Rayleigh–Gans (RG) phase function is preferable. A comparison of the HG, RG and Mie phase functions for scattering parameters corresponding to the aqueous latex particle suspensions used in this study ($x = \pi d/\lambda = 3.477$, $n = 1.193$, $g = 0.8353$) is shown in Fig. 3. It can be seen in Fig. 3 that while the RG phase function more closely matches the Mie phase function, particularly in the important forward directions, there is a substantial deviation at about 80 degrees. Moreover, the expression for the RG phase function is significantly more complicated than the HG function and is not amenable to analytic expression as a cumulative probability function. Thus other means, such as curve-fitting and/or table look-up must be resorted to if the RG phase function is to be used in Monte Carlo computations. Such strategies can as easily be applied to the Mie phase function data as to the RG function.

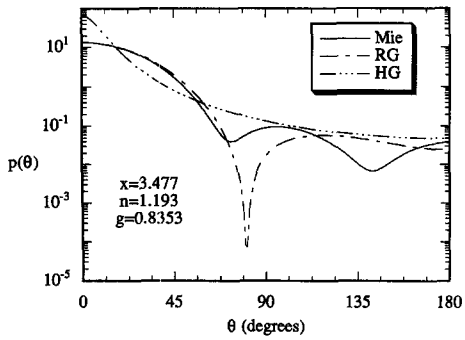

Fig. 3. Comparison of Mie, Heyney–Greenstein and Rayleigh–Gans phase functions for latex particles in water; $x = 3.477$ ($d = 0.653$ μm, $\lambda = 0.784/1.3289$) and $n = 1.5850/1.3289$ ($g = 0.835$).

A brief attempt at this was made using a ninth order polynomial curve fit to the Mie phase function. The results showed only slight differences in R and T at very early times between the Mie curve fit and the HG phase function. Thus, the HG function was used for anisotropic scattering simulations.

The difference between anisotropic and equivalent isotropic time-resolved scattering results is displayed in Fig. 4. Optical conditions are selected to be the same as those of the 10 mm cell with no absorbing dye added (see figure captions for parameters used). These results show that the only differences come at very early times. The transmittance of the equivalent isotropic case rises faster than the actual anisotropic scattering case. The reason is that the artificially low extinction coefficient of the isotropic calculation allows more of a "snake" component [18] to be transmitted than can be compensated for by the isotropic phase function. For long times, anisotropic and equivalent isotropic results are exactly the same and correspond to the curves labelled MC-Iso and MC-Ani in Fig. 5 ($R(10)$ and $T(10)$ in Fig. 2).

Another difference that appears in the results of Fig. 4 has to do with the time-resolution and statistical fluctuation in the two data sets. Both calculations were

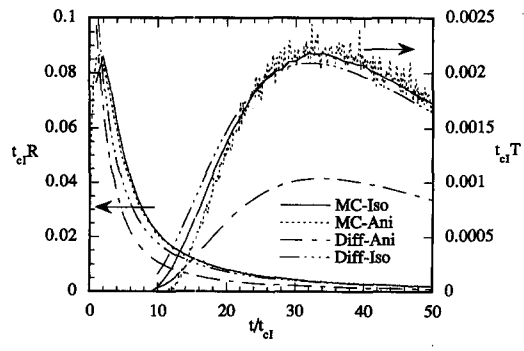

Fig. 4. Short time reflectance and transmittance for slab with plane-wave, pulsed irradiation for both anisotropic and equivalent isotropic scattering by Monte Carlo and diffusion approximation; anisotropic parameters: $\tau = 60$, $\omega = 0.9996$, Heyney–Greenstein phase function with $g = 0.835$; isotropic parameters: $\tau_I = 10$, $\omega_I = 0.9976$.

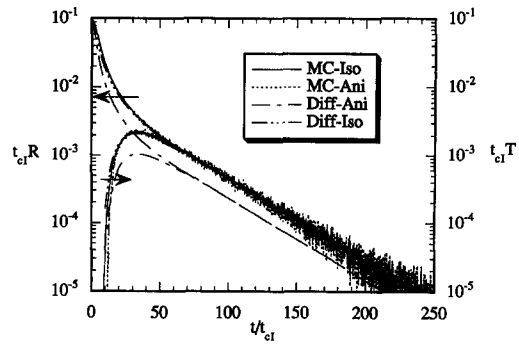

Fig. 5. Long time reflectance and transmittance for slab with plane-wave, pulsed irradiation for both anisotropic and equivalent isotropic scattering by Monte Carlo and diffusion approximation; anisotropic parameters: $\tau = 60$, $\omega = 0.9996$, Heyney–Greenstein phase function with $g = 0.835$; isotropic parameters: $\tau_I = 10$, $\omega_I = 0.9976$.

done with the same number of photon bundles (10^7) and with the same non-dimensional time resolution ($\Delta t' = 1$). However, the characteristic time scales are different between the two cases, with the anisotropic time scale ($t_c = 1/K_e c$) being smaller than the isotropic time scale ($t_{cI} = 1/K_{eI} c$) by a factor of $t_c/t_{cI} = 1 - \omega g$ ($= 0.165$ for the conditions of Fig. 4). In Fig. 4, for easy comparison, reflectance, transmittance and time values are all non-dimensionalized by the same time scale (the isotropic value t_{cI}). As a result, the apparent time resolution is greater in the anisotropic results, as can be clearly seen in the reflectance values. The anisotropic results resolve the reflectance peak much better than the isotropic results do. As a trade-off, the anisotropic results also show a much greater degree of statistical fluctuation in corresponding results at longer times. This is due to the fact that the anisotropic calculation concentrates a larger fraction of the total bundles at shorter times. This effect can be seen in the exaggerated fluctuations of the anisotropic transmission curve. Aside from these cosmetic differences, however, the important result is that the two calculations (isotropic and anisotropic) give nearly identical results over most of the time history, with minor differences arising during the early times of the respective output pulses (reflectance and transmittance).

Figures 4 and 5 also present the corresponding diffusion theory predictions of Ito and Furutsu for the case discussed above. The isotropic case (Diff-Iso) is in good agreement with the Monte Carlo results for both reflectance and transmittance at most times, with only slight disagreement during the early portions of the transmittance rise and more substantial disagreement during the early portion of the reflectance rise. The latter can be attributed to poor convergence of the series representation of the solution. This is more a problem with the series solution than with the diffusion theory itself. It should be noted that other representations of the solution are available, such as equations (46, 47, 49, 50) of ref. [7], which overcome convergence problems at short times but are more

cumbersome. Ten terms were used in calculating the diffusion results of Figs. 4 and 5. Variation of the number of terms showed that the diffusion results were not convergent for $t/t_{cl} < 2$ and $t/t_{cl} < 11$ for R and T, respectively. Nevertheless, the isotropic diffusion results are in good agreement with the Monte Carlo results generally, and match exactly in the long time limit. The anisotropic diffusion results (Diff-Ani), on the other hand, proved to be substantially in error. Over most of the time history the anisotropic diffusion results were lower than the Monte Carlo results by a factor of two. This difference in the anisotropic diffusion results can be traced to the appearance of the lone anisotropic scattering parameter η which appears in the diffusion solution. If the Diff-Ani results are scaled up by a factor of two they match the Monte Carlo results very well. The implication here is that if only normalized results are considered, the apparent error of the diffusion solution is not noticeable. Most comparisons with experimental results are made on a normalized basis. Thus this discrepancy may not be considered to be serious. Nevertheless it is somewhat unsettling. In the absence of an explanation for this disagreement it can only be recommended that the best course to follow for anisotropic diffusion predictions is to use the equivalent isotropic approach (i.e. set $g = 0$ ($\eta = 3$) in those terms of the diffusion solution where η appears alone). As far as the long time reflectance and transmittance values are concerned, the present comparisons with Monte Carlo results would indicate it is appropriate to simplify the expression of Ito and Furutsu to the following one which is a function of only the two isotropic parameters τ_1 and ω_1:

$$t_{cl}R(t_1', \tau_1, \omega_1) = t_{cl}T(t_1', \tau_1, \omega_1) = \omega_1 a_{o1} \exp[-(1-\omega_1)t_1' - 3\omega_1 s_1^2 t_1'/\beta^2]\,; t_1' \to \infty \tag{20}$$

$$a_{o1} = \frac{[(5/6)\beta^2 - s_1^2]s_1^2}{[\beta^3/4 + \beta^2 + \beta s_1^2][s_1^2 + (\beta/3 - s_1^2/\beta)^2]}. \tag{21}$$

5.4. *Effect of detector field-of-view*

The effect of detector field-of-view (fov) on time-resolved reflectance and transmittance results is displayed in Fig. 6. Optical conditions are again selected to be the same as those of the 10 mm cell with no absorbing agent added. The effect of fov is investigated by reducing the output solid angle from the previous cases. In the previous cases, the calculated reflectances and transmittances are hemispherical values; that is, photons are collected over the entire 2π steradian hemisphere in the computation of R and T. Figure 6 shows results in which the collection solid angle is reduced by a factor of 0.024 from 2π to 0.15. This reduction corresponds to a cutoff slab polar angle of $\theta_c = 12.7$ degrees ($\cos\theta_c = 0.9755$) or a numerical aperature (NA) of 0.22, which is the input NA of the detector lens assemblies used in the present experimental study. The narrow fov results have been scaled up to match the hemispherical fov results at long times. Figure 6 shows that the decay rates of both cases match very well. The only differences come at very early times. The reflectance of the hemispherical fov case ($\theta_c = 90°$) rises faster than that of the narrow fov case ($\theta_c = 12.7°$). For long times the hemispherical and narrow fov results are exactly the same and correspond to the curves labelled $R(10)$ and $T(10)$ in Fig. 2 (with appropriate scaling to convert from t_{cl} to t_c).

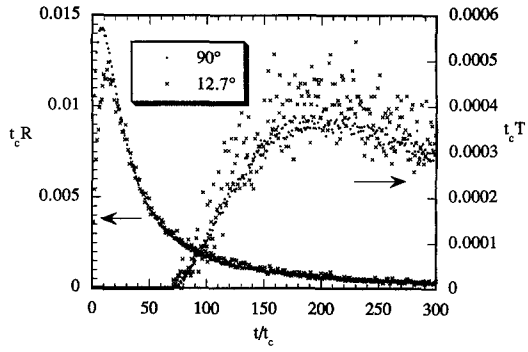

Fig. 6. Monte Carlo time-resolved reflectance and transmittance for slab with plane-wave, pulsed irradiation for both hemispherical ($\theta_c = 90°$) and narrow ($\theta_c = 12.7°$) detector field-of-view; $\tau = 60$, $\omega = 0.9996$, Heyney–Greenstein phase function with $g = 0.835$.

The magnitude of the scaling between the hemispherical and narrow fov cases can be estimated by assuming that the reflected and transmitted intensities are diffuse at all times. In this case the ratio of fluxes between the two cases at any instant of time (or integrated over time) is given by the geometric view factor

$$\frac{2\pi \int_0^{\theta_c} \cos\theta \sin\theta \, d\theta}{2\pi \int_0^{\pi/2} \cos\theta \sin\theta \, d\theta} = 1 - \cos^2\theta_c = 0.048. \tag{22}$$

This ratio indicates that the narrow fov reflectance and transmittance values should be scaled up by a factor of $1/0.048 = 21$ to be comparable with the corresponding hemispherical results. This factor (21) is fairly close to the Monte Carlo calculated ratios of 19 and 16 for the time-integrated reflectance and transmittance values, and 18 and 17 for the long-time values. The fact that the diffuse factor (21) is somewhat greater than the Monte Carlo factors indicates that the transmitted and reflected intensities are higher in the near-normal directions than at the grazing angles. This is consistent with expected behavior for radiation diffusion transport, which propagates energy via a quasi-isotropic intensity distribution that is slightly biased in the direction of the net flux.

6. EXPERIMENTAL SYSTEM

A schematic of the optical system used in this study is shown in Fig. 7. Time-resolved transmittance was

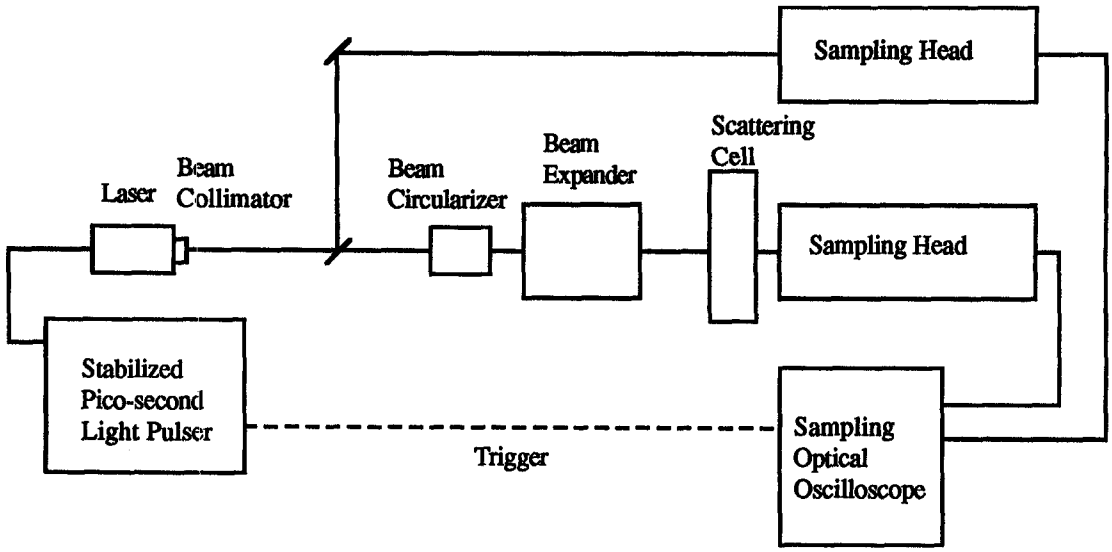

Fig. 7. Schematic diagram of optical system.

measured on aqueous latex particle suspensions in planar scattering cells. A pulsed diode laser ($\lambda_o = 784$ nm, 353 mW) operating at 1 MHz was used in conjunction with an optical oscilloscope to measure the time-dependent transmitted signal. The FWHM of the incident pulse was approximately 50 ps. The laser beam was collimated before splitting off a small fraction as a reference pulse which was used to deconvolute the transmitted pulse signal. The main beam was circularized using an anamorphic prism pair and reduced to a diameter of approximately 1 mm before arriving at the scattering cell. The black, rectangular scattering cells measured 10×10 cm with a 10 mm anti-reflection coated circular window on the front side and a 20 mm anti-reflection coated window on the back side. Two cell thicknesses, 10 and 20 mm, were used. The input numerical aperature of the sampling head detector lens assemblies was 0.22, resulting in a fov half angle of 12.7°. The distance between the detector input lens assembly focal point and the cell back window was 8 mm such that the effective region of photon collection from the cell was a 4 mm diameter circle. Data was collected over a period of 48 h per run to maximize signal-to-noise ratio during the long-time (decay) portion of the transmitted pulse.

The scattering cells were filled with aqueous suspensions of $d = 0.653$ μm diameter polystyrene latex particles (Immutex G0601), density 1.05 g cm^{-3}. The particle refractive index was assumed to be $n_p = 1.5850$ and the absorption index $k_p = 0$. The water optical constants [19] were taken as $n_w = 1.3289$ and $k_w = 1.39 \times 10^{-7}$. The relative particle refractive index was thus $n_p/n_w = 1.1927$ and the wavelength in the aqueous medium was $\lambda = \lambda_o/n_w = 590$ nm. The particle size parameter was $x = \pi d/\lambda = 3.477$. The corresponding Mie scattering properties (assuming a monodispersion of particles and monochromatic light) are $Q_s = 0.8334$ and $g = 0.8353$. The latex solution (10% solids by mass as received) was diluted by 30 times (29 parts water to 1 part solution) to achieve a particle volume fraction of $f_v = 3.14 \times 10^{-3}$. At this loading the average interparticle distance is sufficient for independent scattering to be assumed (the average particle clearance to wavelength ratio is $c/\lambda = 5.7$ which is well above the critical value of 0.5 for the onset of dependent scattering [20]). Neglecting particle size distribution effects, the scattering, absorption and extinction coefficients for the 30× diluted white latex suspension can be calculated as

$$K_s = 1.5 f_v Q_s/d = 6.01\,\text{mm}^{-1}$$

$$K_{sI} = K_s(1-g) = 0.990\,\text{mm}^{-1}$$

$$K_a = 4\pi k_w/\lambda_o = 2.23 \times 10^{-3}\,\text{mm}^{-1}$$

$$K_e = K_s + K_a = 6.0122\,\text{mm}^{-1}$$

$$K_{eI} = K_{sI} + K_a = 0.9922\,\text{mm}^{-1}.$$

The corresponding albedos are $\omega = 0.9996$ and $\omega_I = 0.9977$ and the optical thicknesses for the 10 mm cell are $\tau = 60.12$ and $\tau_I = 9.922$. The characteristic transport times are $t_c = 1/(K_e c) = 0.739$ ps and $t_{cI} = 1/(K_{eI} c) = 4.48$ ps, where $c = c_o/n_w = 0.225$ mm ps^{-1}. The time for direct, ballistic transport across the 10 mm slab is thus $t_o = L/c = \tau_I t_{cI} = 44.44$ ps or $t_o/t_{cI} = \tau_I = 9.922$.

It should be noted that white aqueous latex particle suspensions are often assumed to be non-absorbing in the visible and near infrared regions due to the low absorption coefficient of both water and polystyrene in the visible region. The absorption spectrum of water, however, exhibits a minimum at 500 nm and increases rapidly into both the infrared and ultraviolet regions. As a result absorption by water in the near infrared region may or may not be negligible, depending on the nature of a particular measurement and the

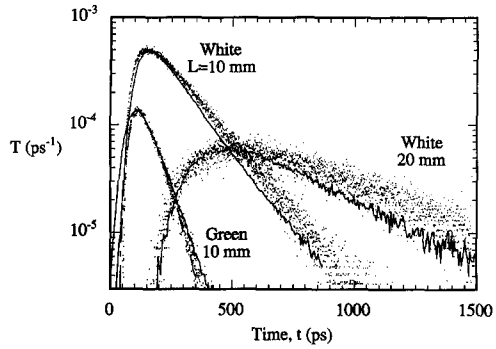

Fig. 8. Time-resolved transmittance: experimental-lines (broken-deconvoluted), Monte Carlo-points. Three cases: white latex 10 mm cell ($\tau = 60$, $\omega = 0.9996$, $g = 0.835$); white latex 20 mm cell ($\tau = 120$, $\omega = 0.9996$, $g = 0.835$); green latex 10 mm cell ($\tau = 60$, $\omega = 0.9920$, $g = 0.835$). Experimental data scaled and time-shifted to match Monte Carlo peak.

desired output. In the case of time-resolved scattering measurements on thick suspensions it is important to include absorption by water absorption. Failure to do so results in major error in one of the most important output pulse parameters, the asymptotic log slope.

In addition to the white latex suspension, a more strongly absorbing suspension was also prepared and tested. Green dye was added to the white latex suspension at a dilution of 400 times to increase the absorption coefficient. Independent tests verified that the dye acted only to increase the absorption coefficient of the continuous medium (water) and did not adhere to or absorb into the particles or alter the particle scattering properties. The absorption coefficient of the diluted dye was measured independently as $K_{a,dye} = 0.0463\ \text{mm}^{-1}$. Thus the optical properties of the green suspension should be slightly modified from those of the white suspension as follows:

$$K_a = K_{a,w} + K_{a,dye} = 0.0485\,\text{mm}^{-1}$$

$$K_e = K_s + K_a = 6.0585\,\text{mm}^{-1}$$

$$K_{eI} = K_{sI} + K_a = 1.0385\,\text{mm}^{-1}.$$

The albedos for the green latex are $\omega = 0.9920$ and $\omega_I = 0.9530$. In terms of albedo, this does not represent a big percentage change from the white latex case but in terms of absorption ($1\text{-}\omega$) it is a relatively big change, enough to significantly modify the scattering behavior. The cell optical thicknesses, at $\tau = 60.59$ and $\tau_I = 10.38$ for the 10 mm cell, are not much changed by the dye.

7. EXPERIMENTAL RESULTS

The results of the experimental time-resolved transmittance measurements are shown in Fig. 8 as lines and Monte Carlo predictions are shown as points. Three cases are presented: white latex 10 mm cell ($\tau = 60$, $\omega = 0.9996$, $g = 0.835$); white latex 20 mm cell ($\tau = 120$, $\omega = 0.9996$, $g = 0.835$); green latex 10 mm cell ($\tau = 60$, $\omega = 0.9920$, $g = 0.835$). The experimental data have been scaled in magnitude and shifted in time to match the peaks of the Monte Carlo results. For the case of the green latex 10 mm cell, both raw (solid line) and deconvoluted (broken line) data are shown while for the two white latex cases only the raw (non-deconvoluted) data are shown. This is because for the two longer pulse cases deconvolution did not significantly change the output pulse shape. Deconvolution had a more significant effect on the shorter output pulse green case, particularly during the rise portion of the pulse. In terms of the long-time portion of the output signals, an important step in the data reduction for all cases was subtraction of the background. Either with or without background subtraction, the signal eventually reaches the noise level and the apparent asymptotic slope always tends toward zero, an incorrect results. Background subtraction extends the range of the correct log–linear decay rate and thus allows collection of a larger range of useful data.

The Monte Carlo simulations were based on the assumptions of plane-wave, Dirac-delta pulse incident radiation at time $t = 0$, hemispherical detection, and no refractive index mismatch at the slab boundaries. In spite of the obvious variation between these assumptions and the actual experimental conditions it can be seen that the Monte Carlo predictions match the experimental pulse shapes very well for all three cases. This agreement is not unexpected given that Monte Carlo simulations show the radially integrated transmitted pulse shape is insensitive to collection geometry (see e.g. Fig. 6). The disagreement which appears between the experimental data and Monte Carlo predictions in the decay portion is probably due to finite beam and finite detection effects. Photons emanating from outside the 4 mm circular region covered by the detector were not detected in this experiment and thus the measured pulse was only a close approximation to the radially integrated value. The effect of this, according to Ito's results [8], would be for the measured pulse to be slightly narrower and steeper in decay than the predicted plane wave pulse, which is consistent with Fig. 8. On the rise portion of the transmitted pulse, signal deconvolution results in better agreement, although this effect is only important for relatively short transmitted pulse conditions, such as the green latex 10 mm cell case.

8. DETERMINATION OF EQUIVALENT ISOTROPIC PROPERTIES

As mentioned previously, one scheme for measuring the unknown optical properties τ_I and ω_I of a thick, turbid medium is to measure two scattered pulse parameters that are functions of τ_I and ω_I. To test this procedure, ALS and RMSW were selected as pulse parameters for use in conjuction with the cor-

responding plane-wave diffusion theory relations obtained by Ito and Furutsu. The RMSW expression of equations (12)–(16) has the parameter limit $\beta y^{1/2} \leqslant 1$. Of the three experimental cases presented in Fig. 8, the white latex 10 mm cell case is closest to satisfying this restriction ($\beta y^{1/2} = 0.85$, using the Mie theory values $\tau_I = 9.922$ and $\omega_I = 0.9976$). Therefore this case is selected as a test case for obtaining τ_I and ω_I from ALS and RMSW. The logarithmic decay rate obtained from linear regression analysis of the experimental data is $m = 0.00303$ ps^{-1} which gives τ_IALS $= 0.310$. The non-dimensional pulse width obtained from numerical integration of the experimental data is RMSW = 3.51. Using these values in the plane-wave diffusion results of Ito and Furutsu to solve for the isotropic optical properties gives $\tau_I = 10.66$ and $\omega_I = 0.9933$. From these isotropic properties and the total optical depth ($\tau = 60.12$) the remaining optical properties can be obtained as follows (see Exp/ALS-RMSW):

with the reference value (0.0022) while the MCA value (0.0007) is low by a factor of three. The Exp/ALS-RMSW value (0.0067) is too big by a factor of three. Part of the reason for this disagreement is the limited accuracy of equation (12). Using the Exp/ALS-RMSW results, the parameter $\beta y^{1/2}$ is 1.5, which is beyond the recommended limit of 1. Since the accuracy of the three-term expansion for RSMW is questionable, consideration was given to using the more general expression for pulsewidth, equation (59) of ref. [7]. While this would also allow comparison for the other two experimental cases of Fig. 8 for which $\beta y^{1/2}$ is larger (approximately 1.7 and 3.8), it would not address the main source of disagreement between experiment and theory (whether Monte Carlo or diffusion) which is the finite-beam, finite-detection effects, as discussed at the end of Section 7. Therefore it is probably of little value to seek better agreement using a more accurate expression for RMSW since no new information stands to be gained. Further

	τ_I	ω_I	g	K_{eI} [mm^{-1}]	K_{sI} [mm^{-1}]	K_a [mm^{-1}]
Exp/ALS-RMSW	10.66	0.9933	0.8237	1.066	1.059	0.0067
Reference	9.922	0.9976	0.8353	0.9922	0.990	0.0022
MCI/ALS-RMSW	10.73	0.9965	0.8220	1.073	1.069	0.0037
MCA/ALS-RMSW	9.023	0.9992	0.8500	0.9023	0.902	0.0007

For comparison, the independently determined properties are also shown. These properties, labelled 'reference', were obtained from Mie theory and time-independent transmission spectroscopy measurements. Generally good agreement is seen between the ALS-RMSW experimentally derived (plane-wave) results and the reference values. The degree of disagreement between these two sets of parameters seems to be consistent with the degree of disagreement between the plane-wave Monte Carlo results and experimental results seen in Fig. 8.

Two additional data sets are presented for comparison, MCI/ALS-RMSW and MCA/ALS-RMSW. These results are obtained from the Monte Carlo calculations for isotropic scattering (MCI, Fig. 2) and anisotropic scattering (MCA, Fig. 8). The logrithmic decay rate is $m = 0.00267$ ps^{-1} for both MCI and MCA, which gives τ_IALS $= 0.2738$. The RMSW values are 3.76 and 3.65 for MCI and MCA, respectively. The difference in these values is due to the difference in the rise time characteristics shown in Fig. 4. Using these values for ALS and RMSW in the plane-wave diffusion results of Ito and Furutsu to solve for the isotropic optical properties gives the property values shown above.

Of the various properties the absorption coefficient shows the largest relative disagreement. The MCI absorption coefficient (0.0037) is in fair agreement

improvement with this technique might only be expected if one or more of the theoretical assumptions (e.g. plane-wave incidence, radially integrated detection, monochromatic light, monodisperse particles, etc.) were either relaxed or matched more closely experimentally.

It should be noted that in obtaining the experimental values of ALS and RMSW, some judgement on which data to include is required. In the above example, for ALS, data for $t < 300$ ps were excluded based on visual inspection of the pulse trace (alternatively some mathematical criterion of convergence to a constant log slope could be applied). In addition, data for $t > 860$ ps were also excluded because the signal is approaching the noise level. Similarly, for RMSW, data for $t > 860$ ps were obtained by extrapolation of the $300 < t < 860$ ps data. It is important to include the long-time data, since it contributes significantly to the integrals in RMSW.

As mentioned in Section 3 there are a variety of output pulse parameters that could be selected to determine the equivalent isotropic properties; here ALS and RMSW were selected. ALS was chosen because of its simple diffusion theory result, its sensitive dependence on albedo, and its ease of measurement. For these reasons ALS would seem to be one that should always be considered. RMSW was chosen because of the simple Ito and Furutsu diffusion theory

result and because it is reasonably linearly independent of ALS over the entire range of albedos and optical thicknesses. The factors which determine parameter choice, then, are simplicity of theoretical representation, ease of measurement and mutual independence. A detailed investigation of various pairs was not done but physical considerations might indicate that the pair t_m and some measure of pulse width (whether FWHM or RMSW) is not as good as some other choices since both t_m and pulse width tend to increase with optical depth and with albedo. As discussed in the introduction, ref. [6] shows that both t_m and FWHM increase linearly with reduced optical thickness above thicknesses of 10. If a similar trend occurred in albedo (as Fig. 8 suggests) then the Jacobian could be small and this pair would not work well.

One final exercise involving the plane-wave diffusion theory results was attempted. This involved trying to see how small the albedo could become and still have reasonably accurate prediction of ALS by the plane-wave diffusion theory results. Comparison with Monte Carlo results indicated that for a semi-infinite slab the Ito and Furutsu expression for ALS was accurate to within 10% for $\omega_1 > 0.5$ as long as the optical depth condition $\tau_1 > 3$ was maintained. Thus it is reasonable to expect that the optical properties of more strongly absorbing media, even $\omega_1 < 0.5$, might be obtainable by the methods discussed above, given that suitable functional relations between output pulse parameters and optical properties were available.

9. CONCLUSIONS

Methods for obtaining optical properties of thick, turbid planar media from time-resolved transmission measurements using pulsed beam irradiation have been considered. Both exact (Monte Carlo) and approximate (diffusion) approaches have been demonstrated. The diffusion method consists of measuring two independent transmitted pulse parameters (such as asymptotic log slope and width) and mathematically inverting to obtain the isotropic scattering and absorption parameters. The scattering asymmetry parameter can then be obtained from a conventional direct, unscattered transmission measurement. This method appears to be especially useful for obtaining relatively quick yet reasonably accurate estimates for properties of unknown systems. More accurate results can be obtained from comparisons with Monte Carlo calculations. Furthermore these methods should be applicable, in principle at least, to more complicated geometries as well as to reflective back-scattering measurements. It was also found that the albedo criterion for application of diffusion theory to time-dependent scattering may be much less restrictive than is usually reported (weak absorption or albedo near one is not necessary).

One important issue that has not been considered here is the effect of nonhomogeneous properties. Non-homogeneity introduces the possibility of obtaining non-unique solutions by the present two parameter approach. Since non-homogeneous properties are a fact-of-life in all naturally occurring systems, this issue needs to be investigated.

Acknowledgements—This work was made possible by support from the U.S. National Science Foundation (INT-9201118) and the Agency of Industrial Science and Technology (AIST-MITI) of Japan. The assistance of Ms Yukari Takahashi in setting up the optical system is gratefully acknowledged.

REFERENCES

1. B. Chance, J. S. Leigh, H. Miyake, D. S. Smith, S. Nioka, R. Greenfield, M. Finander, K. Kaufmann, W. Levy, M. Young, P. Cohen, H. Yoshioka and R. Boretsky, Comparison of time-resolved and -unresolved measurements of deoxyhemoglobin in brain, *Proc. Natnl. Acad. Sci. U.S.A.* **85,** 4971–4975 (1988).
2. B. Wilson, Y. Park, Y. Hefetz, M. Patterson, S. Madsen and S. Jacques, The potential of time-resolved reflectance measurements for the noninvasive determination of tissue optical properties. In *Thermal and Optical Interaction with Biological and Related Composite Materials* (Edited by M. J. Berry and G. M. Harpole), *Proc. SPIE*, Vol. 1064, pp. 97–106 (1989).
3. M. Essenpreis, C. E. Elwell, M. Cope, P. van der Zee, S. R. Arridge and D. T. Delpy, Spectral dependence of temporal point spread functions in human tissues, *Appl. Opt.* **32,** 418–425 (1993).
4. M. S. Patterson, B. Chance, and B. C. Wilson, Time resolved reflectance and transmittance for the non-invasive measurement of tissue optical properties, *Appl. Opt.* **28,** 2331–2336 (1989).
5. S. J. Madsen, B. C. Wilson, M. S. Patterson, Y. D. Park, S. L. Jacques and Y. Hefetz, Experimental tests of a simple diffusion model for the estimation of scattering and absorption coefficients of turbid media from time-resolved diffuse reflectance measurements, *Appl. Opt.* **31,** 3509–3517 (1992).
6. G. Zaccanti, P. Bruscaglioni, A. Ismaelli, L. Carraresi, M. Gurioli and Q. Wei, Transmission of a pulsed thin light beam through thick turbid media: experimental results, *Appl. Opt.* **31,** 2141–2147 (1992).
7. S. Ito and K. Furutsu, Theory of light pulse propagation through thick clouds, *J. Opt. Soc. Am.* **70,** 366–374 (1980).
8. S. Ito, Theory of beam light pulse propagation through thick clouds: effect of beam width and scatterers behind the light source on pulse broadening, *Appl. Opt.* **20,** 2706–2715 (1981).
9. P. P. Ho, P. Baldeck, K. S. Wong, K. M. Yoo, D. Lee and R. R. Alfano, Time dynamics of photon migration in semiopaque random media, *Appl. Opt.* **28,** 2304–2310 (1989).
10. K. M. Yoo and R. R. Alfano, Time-resolved coherent and incoherent components of forward light scattering in random media, *Opt. Lett.* **15,** 320–322 (1990).
11. A. Ishimaru, *Wave Propagation and Scattering in Random Media*, Vol. 1, p. 180. Academic Press, New York (1978).
12. S. T. Flock, B. C. Wilson and M. S. Patterson, Total attenuation coefficients and scattering phase functions of tissues and phantom materials at 633 nm, *Med. Phys.* **14,** 835–843 (1987).
13. B. C. Wilson and G. Adam, A Monte Carlo model for the absorption and flux distributions of light in tissue, *Med. Phys.* **10,** 824–830 (1983).
14. K. Furutsu and Y. Yamada, Diffusion approximation

in a heavily dissipative medium, submitted to *Phys. Rev. Lett.*
15. Y. Yamada and Y. Hasegawa, Time-dependent FEM analysis of photon migration in random media, *Proc. SPIE* **1888,** 167–178, (1993).
16. J. Haselgrove, J. Leigh, Y. Conway, N-G. Wang, M. Maris and B. Chance, Monte Carlo and diffusion calculations of photon migration in non-infinite highly scattering media. In *Time-resolved Spectroscopy and Imaging of Tissues* (Edited by B. Chance and A. Katzir), *Proc. SPIE*, Vol. 1431, pp. 30–41 (1991).
17. R. Graaff, J. G. Aarnoudse, F. F. M. de Mul and H. W. Jentink, Light propagation parameters for anisotropically scattering media based on a rigorous solution of the transport equation, *Appl. Opt.* **28,** 2273–2279 (1989).
18. L. Wang, P. P. Ho, C. Liu, G. Zhang and R. R. Alfano, Ballistic 2-D imaging through scattering walls using an ultrafast optical Kerr gate, *Science* **253,** 769–771 (1991).
19. G. M. Hale and M. R. Querry, Optical constants of water in the 200-nm to 200-μm wavelength region, *Appl. Opt.* **12,** 555–563 (1973).
20. M. Q. Brewster, *Thermal Radiative Transfer and Properties*, pp. 332–335. Wiley, New York (1992).